Spectral Dependence of Light Exposure on Retinal Pigment Epithelium Disruption in Living Primate Retina

Jie Zhang,[1,2] Ranjani Sabarinathan,[1] Tracy Bubel,[1] Wuao Jia,[3] David R. Williams,[1,3–5] and Jennifer J. Hunter[1,3–6]

[1]Center for Visual Science, University of Rochester, Rochester, New York, United States
[2]Robotrak Technologies, Nanjing, Jiangsu, China
[3]The Institute of Optics, University of Rochester, Rochester, New York, United States
[4]Flaum Eye Institute, University of Rochester, Rochester, New York, United States
[5]Department of Biomedical Engineering, University of Rochester, Rochester, New York, United States
[6]School of Optometry and Vision Science, University of Waterloo, Waterloo, Ontario, Canada

Correspondence: Jennifer J. Hunter, 200 Columbia St. W, University of Waterloo, Waterloo, ON N2L 3G1, Canada;
jjhunter@uwaterloo.ca.

Received: February 28, 2023
Accepted: November 21, 2023
Published: February 28, 2024

Citation: Zhang J, Sabarinathan R, Bubel T, Jia W, Williams DR, Hunter JJ. Spectral dependence of light exposure on retinal pigment epithelium disruption in living primate retina. *Invest Ophthalmol Vis Sci.* 2024;65(2):43. https://doi.org/10.1167/iovs.65.2.43

Purpose. RPE disruption with light exposures below or close to the American National Standards Institute (ANSI) photochemical maximum permissible exposure (MPE) have been observed, but these findings were limited to two wavelengths. We have extended the measurements across the visible spectrum.

Methods. Retinal imaging with fluorescence adaptive optics scanning light ophthalmoscopy (FAOSLO) was used to provide an in vivo measure of RPE disruption at a cellular level. The threshold retinal radiant exposures (RREs) for RPE disruption (localized detectable change in the fluorescence image) were determined at 460, 476, 488, 530, 543, 561, 594, 632, and 671 nm (uniform 0.5° square exposure) using multiples locations in 4 macaques.

Results. FAOSLO is sensitive in detecting RPE disruption. The visible light action spectrum dependence for RPE disruption with continuous wave (CW) extended field exposures was determined. It has a shallower slope than the current ANSI blue-light hazard MPE. At all wavelengths beyond 530 nm, the disruption threshold is below the ANSI blue-light hazard MPE. There is reciprocity of exposure irradiance and duration for exposures at 460 and 594 nm.

Conclusions. We measured with FAOSLO the action spectrum dependence for photochemical RPE disruption across the visible light spectrum. Using this in vivo measure of phototoxicity provided by FAOSLO, we find that thresholds are lower than previously measured. The wavelength dependence in our data is considerably shallower than the spectral dependence of the traditional ANSI blue-light hazard, emphasizing the need for more caution with increasing wavelength than expected.

Keywords: fluorescence adaptive optics scanning light ophthalmoscopy (FAOSLO), retinal pigment epithelium (RPE) disruption

The absorption of light is a necessary first step to seeing, but too much light can cause injury to the retina and the underlying structures.[1–5] Light can result in damage through various mechanisms, such as photothermal, photomechanical, and photochemical effects. Photochemical injury is a commonly observed mechanism for light induced retinal damage, such as solar retinopathy, welder's maculopathy, operation microscope toxicity, and endoilluminator toxicity.[6–9] Photochemical damage occurs at ultraviolet and visible wavelengths and tends to appear with longer duration exposures where it is not masked by other forms of damage, such as thermal. Under relatively ambient conditions, photochemical damage has a potential role in chronic retinal damage throughout life and may be linked to retinal degenerative diseases, such as age-related macular degeneration (AMD).[10,11]

Retinal imaging with a fluorescence adaptive optics scanning light ophthalmoscope (FAOSLO) provides an in vivo cellular scale measure of light-induced changes. It can noninvasively reveal cellular level changes in photoreceptor and RPE layers. The unique autofluorescence (AF) property of lipofuscin granules accumulated in the cytoplasm of RPE cells makes imaging possible. The RPE mosaic appears as a pattern of cells with dark centers likely including the cell nuclei, and brighter fluorescent surrounds from the lipofuscin granules located in the cytoplasm of the cells.[12] At light levels that were previously thought to be safe, Morgan et al. discovered using FAOSLO 2 changes in AF images of the RPE following long duration uniform exposure to 568 nm light in macaque.[13,14] The first was an immediate reduction in lipofuscin AF that recovers in several hours. This RPE AF reduction was observed with exposures two orders of magnitude

below the maximum permissible exposure (MPE) for the American National Standards Institute (ANSI) standard at that time.[15] The other phenomenon was characterized by a disruption in the appearance of the lipofuscin distribution of the RPE mosaic. This RPE disruption is defined as any detectable structural change from the pre-exposure condition of the cell mosaic in the exposed region relative to the corresponding mosaic in the immediately surrounding area. RPE disruption does not appear immediately following the exposure. RPE disruption was observed at irradiances that were approximately 3 times below the ANSI Z136.1-2007 standard. In addition, Hunter et al. observed RPE disruption at 488 nm for light exposures below previously published damage thresholds.[16] The appearance of RPE disruption at light levels that were previously thought to be safe raised concerns that the ANSI Standard and other safety guidelines may provide insufficient protection for specific cases of long duration intentional uniform exposures. In response, the ANSI Z136.1-2014 standard applied highly restrictive limits for intentional long-duration ophthalmic exposures as a temporary interim solution.[17] These observations underscore the need to accurately measure the damage action spectrum. To address these concerns, we determined the threshold for photochemical RPE disruption in macaques for 9 wavelengths across the visible spectrum from 460 nm to 671 nm. We utilized the FAOSLO imaging of RPE AF to determine the threshold for RPE disruption across the visible spectrum.

Methods

Animal Preparation

Thresholds for RPE disruption were determined using eight eyes from four macaques. Table 1 provides information about each monkey. Animals were handled in accordance with a protocol approved by the University of Rochester's Committee for Animal Research and in adherence with the ARVO Statement for the Use of Animals in Ophthalmic and Vision Research.

During imaging and light exposure, macaques were sedated using ketamine (10–20 mg/kg) and valium (0.25 mL/kg). Pupils were dilated and cyclopleged with one drop each of phenylephrine hydrochloride (2.5%) and tropicamide (1%). For FAOSLO imaging, macaques were then intubated and maintained under anesthesia with isoflurane (1.0–5.0%). To reduce involuntary eye-drifts, the paralytic dose of vecuronium (20–50 µg/kg/hour), was administered for a maximum period of 6 hours. Breathing was maintained with a ventilator. During anesthesia, heart rate, O_2, CO_2, blood pressure, and anal temperature were monitored at 15-minute intervals. The body temperature was maintained between 36.7 and 39.4°C using a heating pad. A lid speculum held the eye open for imaging, and a rigid gas permeable contact lens coated with Genteal (Alcon, Fort Worth, TX, USA) was used to correct for base refractive error and maintain corneal hydration for the duration of each experiment. The pupil of the imaged eye was aligned with the imaging system by a head post rotation mount and a three-axis translation stage, or a five-way motorized stereotaxic cart. Light was directed to different retinal locations by adjusting the angle of rotation of the animal's head relative to the optical system.

Fluorescence Adaptive Optics Scanning Light Ophthalmoscope

A custom FAOSLO designed and built to achieve dual channel (reflectance and fluorescence) retinal imaging in the living monkey eye has been described previously.[18] An 843 nm laser diode (QFLD-850–75S; QPhotonics) provided approximately 20 µW of light for measuring the eye's aberrations with a Shack-Hartmann wavefront sensor. A deformable mirror (DM 97-15; ALPAO, France) was used in closed loop to correct the aberrations and adjust the retinal plane in focus.[19–21] Two 2° square field of view images were captured simultaneously at a 26.5 Hz frame rate. One was a reflectance image of the cone mosaic using approximately 200 µW of 794 nm light from a superluminescent diode (S-790-G-I-15 Broadlighter; Superlum, Ireland) captured through a 1.8 Airy disk diameter pinhole onto a PMT (H7422-50; Hamamatsu, Japan). The second was a fluorescence image of the RPE mosaic using 20 to 40 µW from a 561 nm laser diode (iChrome MLE-LFE; Toptica Photonics, Germany) for excitation and emission collected in the range of 624 ± 20 nm (FF01-620/40-25; Semrock) through a 2 Airy disk diameter pinhole onto a PMT (H7422-40; Hamamatsu, Japan). The gain of the fluorescence channel was set to fully use the dynamic range of the system without saturating pixel intensity. By offsetting the vergence of the 561 nm source to compensate for the longitudinal chromatic aberration in the eye, light reflected from photoreceptors and AF from RPE cells were imaged simultaneously. Motion traces from the high signal-to-noise (SNR) photoreceptor images were used to register the low SNR fluorescence images.[12] Each RPE image is the average of 1300 individual fluorescence frames.

Uniform Light Exposure

Prescribed light exposures were delivered to the retina via an additional Maxwellian view channel on the FAOSLO that bypassed the scanning and adaptive optics. Nine wavelengths between 460 nm and 671 nm were tested: 460, 476, 488, 530, 543, 561, 594, 632, and 671 nm. An Ar/Kr laser (643-AP-A01; Melles Griot, Rochester, NY, USA) was

Table 1. Macaque Information

Macaque #	Species	Age	Sex	Weight (kg)	Axial Length (mm)	Exposure Wavelengths Tested (nm)
1	Macaca fascicularis	7	M	7.9	OD 18.06 OS 18.34	460, 476, 488, 632, 671
2	Macaca mulatta	10	F	5.8	OD 19.96 OS 19.72	460, 476, 530, 561*, 594, 671
3	Macaca fascicularis	6	M	4.3	OD 17.24 OS 17.09	488, 476, 530, 543, 594, 632, 671
4	Macaca fascicularis	15	M	10.4	OD 17.53 OS 17.33	488, 530, 543, 671
5†	Macaca fascicularis	6	M	4.9	OD 17.55 OS 17.56	460, 594
6†	Macaca fascicularis	4	F	3.0	OD 17.88 OS 17.87	460, 594

* This wavelength was only tested in one macaque because we have limited access to another 561 nm laser for FAOSLO imaging.
† Exposures in these macaques were not used for threshold determination but were only used for reciprocity testing.

Investigative Ophthalmology & Visual Science

Table 2. For Each Wavelength, the Retinal Radiant Exposures are Determined From the Exposure Power and Duration for an Assumed Macaque Eye With a Focal Length of 15 mm

λ (nm)	Radiant Exposure (J/cm²)	Power (μW)	Duration (s)	λ (nm)	Radiant Exposure (J/cm²)	Power (μW)	Duration (s)	λ (nm)	Radiant Exposure (J/cm²)	Power (μW)	Duration (s)
460	17	83	35	**488**	17	21	138	**594**	246	59	709
	24	12	329			12	236			136	300
		29	141		24	14	288		257*	500	88
	29*	10	497			40	100			1010	44
		20	249		48	14	587			2040	22
		50	99			42	196		267*	46	1000
		114	43	**530**	49	20	420			92	500
		227	22		70	30	399			114	400
		451	11			65	184			490	94
		563	9			80	150			1000	46
	33*	548	10		99	65	260			2000	23
		227	25			80	212			2280	20
		451	12			100	169		310*	500	106
		550	10	**543**	49	43	196			1000	53
	34	29	200		69	50	235			1450	37
		140	42			156	76			1660	32
	36*	10	624		98	60	280		348	98	608
		20	312			88	191			136	438
		50	125		138	77	307		491	70	1202
	48	15	563	**561**	152	48	543			136	618
476	25	4	1127		215	48	768	**671**	3394	257	2262
		11	384		303	48	1082			282	2100
	36	4	1418	**632**	903	235	658			290	2005
		32	191		1275	228	958		4794	274	2998
		33	187			283	772			347	2367
	51	11	794		1801	200	1542		6772	286	4057
		32	271			283	1090			405	2822
									9565	274	5982
										310	5287

* Data were not used to determine thresholds but were included in reciprocity assessments.

For the purposes of this table, values are rounded to the nearest integer. However, delivered retinal radiant exposures were accurate to within ±5%. Variations in exposure power were occasionally the consequence of reduced system input for a given imaging occasion. A larger number of exposure power and duration combinations were used to confirm reciprocity specifically using 460 nm and 594 nm exposures.

used for the 476 and 530 nm exposures. Six stand-alone fiber-coupled solid-state lasers (MDL-E-460, MGL-III-543, MGL-III-594, MRL-FN-671, CNIlaser, China; iChrome MLE-LFE, Toptica Photonics, Germany; iFLEX-Mustang, Qioptiq, Germany) were used for 460, 488, 543, 561, 594, and 671 nm exposures. A Helium Neon laser was used for the 632 nm exposures. All lasers were fiber coupled into the uniform exposure channel. A computer-controlled motorized shutter aligned with the exposure beam allowed precise control of the exposure duration. The optical elements in this exposure channel were in a 4f configuration (input at the primary focal point of the first optical element is a finite conjugate to the output at the secondary focal point of the second optical element) as described previously.[14] Light was collimated with a 100 mm focal length lens. Assuming a Gaussian beam profile, only the central part of the beam with intensity greater than 96% of the peak was permitted through a mask 3.5 mm square. A 400 mm focal length lens was used to focus the light into the pupil of the eye. The exposure beam was combined with the FAOSLO system just prior to the final fold mirror using a 92/8 pellicle beamsplitter (BP208; Thorlabs, USA). The uniform exposure illuminated a 0.5° square field of view within the 2° FAOSLO imaging area on the retina. To ensure that there were not substantial temperature increases and to prevent thermal damage within the exposure areas, we used laser powers for all wavelengths well below ANSI thermal limits at the cornea.[17] Laser power at the cornea and the exposure duration together were used to define the retinal radiant exposure (RRE) of the 0.5° square exposure area to within ±5%. During each uniform exposure, simultaneous 2° field of view reflectance imaging and wavefront sensing were carried out to facilitate monitoring and compensation of any eye drift by manually adjusting the macaque's head position to cancel any eye movements except the pulsing from the heartbeat and respiration, which was less than approximately 0.1° in any direction. The imaging and exposure locations are typically 8° to 20° eccentric to the fovea. Exposure location was chosen to avoid any overlapping with blood vessels for better RPE disruption characterization. Table 2 summarized the parameters for exposure delivery.

Exposure Delivery and Assessment

The same experimental protocol was followed for each individual exposure. Using the FAOSLO, pre-exposure images of the RPE cells and cone photoreceptors were acquired. The retina was then exposed to a prescribed RRE. If the

eye motion could not be stabilized because of large drifts, the exposure location was abandoned and a new exposure location was found. Immediately after each exposure, cone reflectance and RPE fluorescence images of the same area were captured. The image acquisition software automatically recorded the pre- and immediately post-images as well as reflectance recording throughout the exposure. Infrared reflectance imaging during the exposure allowed precise monitoring of the exposure location for stabilization. A simultaneously recorded fluorescence video identified the location of the exposure region within the imaging field and identified when a system controlled shutter automatically opened and closed to provide precise control of the exposure duration. Follow-up photoreceptor and RPE images were acquired 2 and 4 weeks following exposure. Some exposures were imaged at longer follow-ups to 10 months. In addition to FAOSLO, fundus photography, confocal scanning laser ophthalmoscopy (cSLO) and optical coherence tomography (OCT; Spectralis HRA+OCT; Heidelberg Engineering, Heidelberg, Germany) were performed on each animal prior to delivery of any intentional light exposures and at various time points following exposure. For cSLO, this instrument has four imaging modalities: infrared (IR) reflectance, blue-light reflectance, blue-light autofluorescence, and infrared autofluorescence (IRAF).

Threshold Determination

The initial RRE tested for each wavelength (λ) was based on a logarithmic fit to the midpoints between RREs showing no retinal changes and those demonstrating RPE disruption from previously published 488 nm[16] and 568 nm[14] data (Supplementary Fig. S1).

$$\log\left(RRE\left[J/cm^2\right]\right) = 0.0109\lambda\,[nm] - 3.7832 \qquad (1)$$

A focal length of 15 mm was assumed for all calculations of the RRE.[14] Each starting RRE at a specific wavelength was repeated at four different retinal locations which were randomized in retinal eccentricity in a single animal. The time of day within the 6-hour imaging session for each wavelength and eccentricity were also randomized. Visual inspection of the RPE and photoreceptor images at 2 and 4 weeks post-exposure determined the next RRE tested. If no RPE disruption was detected, then the RRE was increased by 0.3 log units. If RPE disruption or photoreceptor changes were visible, then the RRE was decreased by 0.3 log units. For each wavelength, the same monkey was used to test the second RRE in four new locations at random retinal eccentricities. Again, based on qualitative evaluation, the subsequent RRE was either increased (no RPE disruption at previous step) or decreased (RPE disruption at previous step) by a step of 0.15 log units. This was repeated until bounding RREs with and without RPE disruption or photoreceptor changes were observed. Figure 1 depicts a typical decision diagram for 594 nm light exposure. An additional one to two monkeys were exposed to these bounding RREs to confirm the findings.

Evaluation of RPE Disruption

Cellular level microscopic structural changes visible with the FAOSLO were used to define the presence or absence of light-induced retinal changes in an in vivo monkey model. The RPE disruption threshold was determined by comparing the 4 weeks follow-up RPE images with the pre-exposure images. For each retinal location, the 4 weeks post-exposure RPE image was aligned with respect to the pre-exposure image and the area of the exposure marked using 4 dots at the corners. We had people who were masked to wavelength, monkey, and RRE identify RPE disruption using two different methods. First, 10 people evaluated the images using a 2-alternative forced choice (2AFC) task. Second, 4 out of the above 10 graders evaluated the same set of images using a yes/no task.

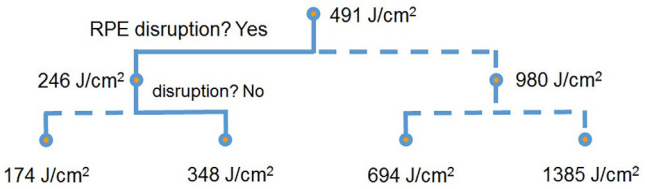

Figure 1. Staircase diagram for RRE threshold determination with 594 nm exposure. Actual testing RREs are *highlighted with solid lines* and other potential testing RREs were also shown.

2AFC Task. In the 2AFC test, the graders were simultaneously presented with the RPE images from a single location in the retina. The left/right positions of the pre- and post-exposure images were randomized. The grader was asked to indicate which image was the post-exposure image. To help maintain attention, audio feedback was provided. The dataset, consisting of all the RPE image pairs of specific exposure wavelength and RRE, was displayed in a random order. Each grader repeated the analysis on the complete dataset eight times. Chance performance on this task corresponds to 50% correct, indicating that the graders could not identify which image was the post-exposure image. We defined the threshold for detection of RPE disruption as 75% correct performance based on the cumulative responses of all trials in all graders.

Yes/No Task. In some circumstances, perceptible differences existed between the two images, such as sharpness or noise, which allowed them to be distinguished even if the grader could not observe RPE disruption. This poses a problem for the 2AFC approach, because a grader's selection of which image is the post-exposure image can be influenced by extraneous factors unrelated to a retinal change produced by the light exposure. To check that this was not corrupting the measured thresholds, we also performed a yes/no task, which explicitly asks the grader whether RPE disruption is visible in the image. The graders were repeatedly (2 Hz refresh rate) presented with the pre- and post-exposure RPE images from a single location in the retina until a decision was made. Using a handheld game controller, the grader was asked to identify if there was RPE disruption in the post-exposure RPE images. The dataset, consisting of all the RPE image pairs of specific exposure wavelength and RRE, was displayed in a random order. Each grader repeated the analysis on the dataset eight times. In the yes/no task, we obtained the percentage of responses with RPE disruption. The threshold is defined as 50%, which means any location with >50% threshold based on the cumulative responses of all trials in all graders had RPE disruption.

Investigative Ophthalmology & Visual Science

RPE Disruption Threshold

After the evaluation, whether 2AFC or yes/no, each individual location was labeled as with or without RPE disruption (as described above). For a given exposure wavelength and RRE, the fraction of exposure locations determined to show RPE disruption was calculated. This is then plotted and the data fit with a probit curve for threshold determination. For all 9 wavelengths, from the plot of percentage of cases showing photochemical RPE disruption versus RREs, the threshold disruption level was determined as the 50% threshold using a probit regression of the dose-response curve. The dose-response function is:

$$y = A1 + \frac{A2 - A1}{1 + 10^{(x_0 - x)p}} \quad (2)$$

where, *A1* is the bottom asymptote, *A2* is the top asymptote, x_0 is 50% threshold, and p is the Hill slope.

Reciprocity

Reciprocity was assessed by varying the power at the cornea and the exposure duration while total RREs remain constant. At 460 and 594 nm, constant RREs with different pairs of duration and irradiance were tested (see Table 2). Threshold determination of RRE for RPE disruption was based on the assumption of a 15 mm focal length emmetropic eye. To determine irradiance, we divided the input power by the exposed retinal area of the eye with an assumed focal length of 15 mm. Considering that axial length variation will affect actual exposure level and reciprocity, the true exposure areas were also used to calculate irradiance. The actual exposed areas were calculated by:

$$Exposure\ Area\ (cm^2) = \left(0.5\ deg \times 291.2\ \mu m/deg \times \frac{L}{24.2\ mm}\right)^2 \quad (3)$$

where L is the measured axial length of tested macaques, 291.2 µm/deg is based on the Le Grand human model eye with axial length of 24.2 mm. At least 5 graders determined whether there was RPE disruption as assessed by 2AFC (described above).

Results

Action Spectrum for RPE Disruption

Visible RPE disruption was observed for some exposures at every wavelength across the visible spectrum between 460 nm and 671 nm, as shown in Figure 2. RPE cell mosaic remained unchanged in the surrounding area. We observed RPE disruption at the site of exposure starting at the first follow-up taken 2 weeks post-exposure. The area of RPE disruption is smoother-edged than the square exposure, no doubt partially due to eye movements during exposure.

For each wavelength, the probit curve was used to determine the 50% threshold based on the 2AFC and yes/no grading. Both grading methods showed a similar trend, except that the yes/no tests had a slightly higher (around 15%) threshold compared with the 2AFC method. A comparison of thresholds obtained using 2AFC and yes/no test is shown in Figure 3. If the retinal radiant exposures were adjusted based on the axial length of the individual primates rather than an assumption of a 15 mm focal length eye, the 2AFC thresholds were also higher (around 20% to 40%). For the remaining threshold analysis, we adopted the more conservative 2AFC results with an assumption of a 15 mm focal length as the threshold to best protect the retina from photochemical RPE disruption due to light exposure. We summarize the 50% RPE disruption thresholds for wavelengths tested in Table 3.

Photochemical RPE Disruption After 671 nm Continuous Wave Laser Exposure

Photochemical retinal damage was thought to occur only with $\lambda < 600$ nm.[22] Figure 4 shows the mosaic of the RPE cells before exposure, 2 and 4 weeks following the exposure from monkey #2, obtained in vivo using the FAOSLO. At 6772 J/cm^2 (see Fig. 4c), long term imaging showed RPE disruption by visual inspection. Therefore, we tested the RRE 0.3 log unit less (3394 J/cm^2) and observed no long-term RPE disruption (see Fig. 4a). Increasing the RRE by 0.15 log units to 4794 J/cm^2 resulted in subtle RPE disruption at the exposure site (see Fig. 4b). These results were confirmed in a different monkey eye. Based on the 2AFC results, the threshold for RPE disruption from 671 nm exposure was 4691.5 J/cm^2. With RREs above threshold, the extent of RPE disruption increased with increasing exposure level.

Long-Term Photoreceptor Loss and RPE Disruption at 460 nm

Although we observed RPE disruption at the higher RREs for all 9 wavelengths tested, the photoreceptors remained unchanged, except for the 460 nm exposures. Figure 5 shows the RPE images and the corresponding photoreceptor mosaic before exposure, 2 weeks, 8 weeks, and 18 weeks after the exposure. At 2 weeks, dark cones were observed at the site of exposure. Cone loss was then observed starting at 8 weeks and was further confirmed at 18 weeks follow-up. Enlarged rod photoreceptors with diameters 3 ± 0.4 µm took over the positions of disrupted cones. Further investigation of the structural change at 10 months following the exposure by confocal, offset pinhole, and fluorescent imaging shows long-term disruption of the RPE layer and cone outer and inner segments disruption, as shown in Figure 6.

FAOSLO is Sensitive in Detecting RPE Disruption

We used a custom in vivo FAOSLO that allows us to accurately determine the threshold for RPE disruption. In addition to FAOSLO, cSLO and OCT images of the retina were obtained on each animal prior to delivery of any intentional light exposures and at various time points following exposure.[23,24]

The OCT data collected at the 0.5° exposure location can be used to test whether the exposure had an effect on photoreceptors or RPE. The approach was described in detail by Masella et al.[25] We compared the OCT data before and after 594 nm exposure, and no measurable changes were detected at testing RREs (maximum RRE tested was typically within 2-fold of the disruption threshold). Therefore, the OCT approach could not provide

Investigative Ophthalmology & Visual Science

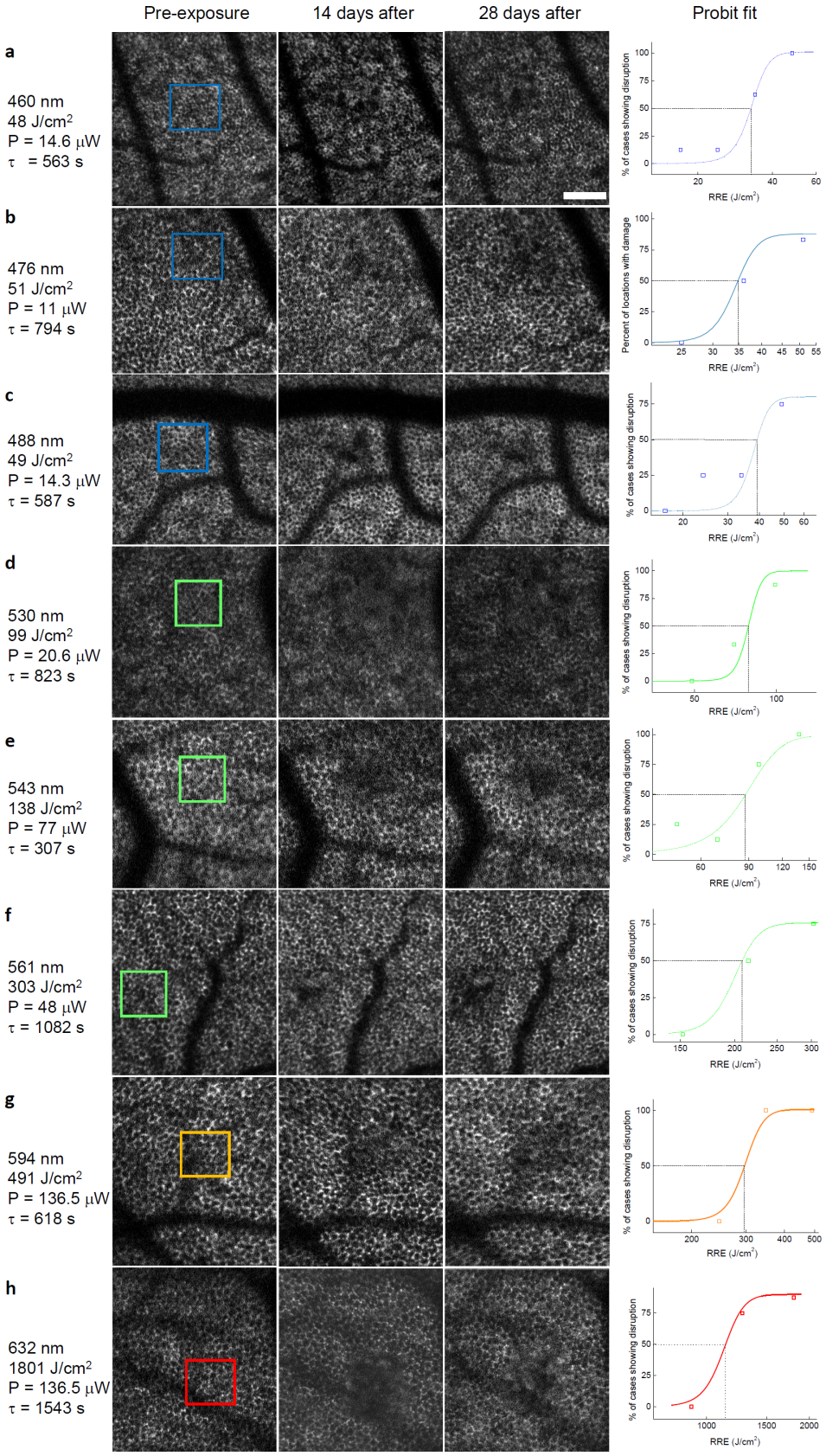

Figure 2. Pre-, 14, and 28 days post-exposure images of the RPE cells in locations exposed above threshold for uniform light exposure field at 460, 476, 488, 530, 543, 561, 594, and 632 nm. The squares in the first column depict the exposure locations inside the 2° imaging area. In the *last column*, corresponding probit curves were shown for each wavelength, indicating the 50% threshold. For all the RRE at these wavelengths, RPE disruption was observed starting at 2 weeks post-exposure. Scale bar = 100 μm. The 671 nm data were shown in Figure 4 separately.

Investigative Ophthalmology & Visual Science

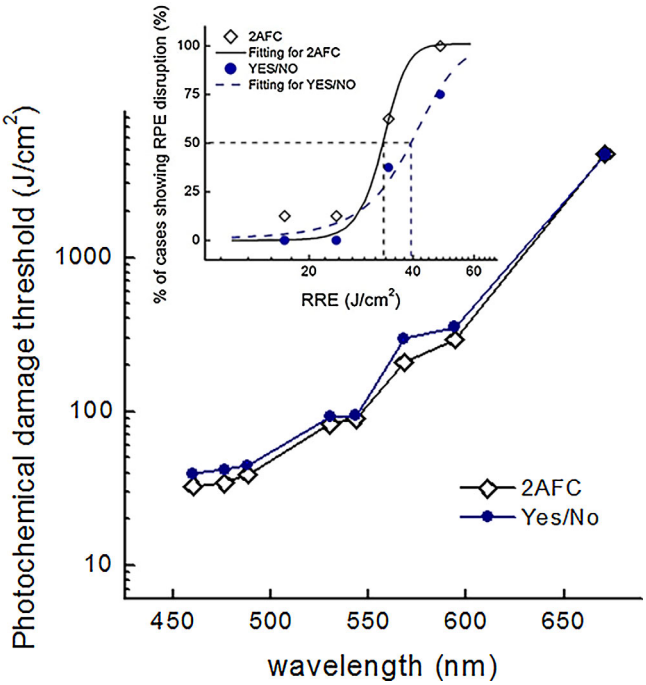

Figure 3. Measured action spectra based on two different evaluation methods: 2AFC and yes/no. *Inset* shows the 50% threshold determination using two methods at 460 nm exposure.

a sensitive enough measure of the photochemical RPE disruption.

Blue-light AF can be used for RPE disruption evaluation due to the unique fluorescent property of the RPE lipofuscin. Typically, visible changes caused by RPE disruption would result in AF signal loss which is usually more than 15% decrease of the mean pixel value within the exposure region.[14] We tested the AF reduction based on blue light AF images of all the tested eyes. With RREs above but within 0.15 log unit of the threshold, 35% of the locations have > 15% mean pixel value drop. With RREs 0.15 log unit higher than the threshold, 67% of the locations show mean pixel value drop in the blue light AF images. Figure 7 gives a typical example of the intensity drop in blue-light AF image from monkey #2 OS after the 594 nm exposure with testing RREs of 491 J/cm^2 (location 1-4), 980 J/cm^2 (location 5), 348 J/cm^2 (location 10–13), and 246 J/cm^2 (location 6-9). We observed blue-light AF decrease within the 2° imaging field, at the sites of exposure to 491 J/cm^2 and 980 J/cm^2. The mean pixel value of the exposure area dropped more than 15% for all 5 locations. However, the mean pixel value remained unchanged and no visible changes were observed at the other 8 locations with RRE level below 348 J/cm^2. We note that long-term RPE disruption was observed at the site of 348 J/cm^2 by FAOSLO, which has a more sensitive measure than cSLO and OCT.

Reciprocity

To test for reciprocity of laser power and duration, additional exposures were tested in monkeys #5 and #6 after the thresholds were established. Plots of irradiance versus exposure duration were generated for both a standard model eye (Figs. 8a, 8b) and accounting for specific axial lengths (Figs. 8c, 8d). The 50% threshold is that provided in Table 3 assuming a 15 mm focal length emmetropic eye.

As shown in Figure 8, the data points representing 0% to 30% occurrence of RPE disruption are distributed near or below the 50% threshold line; the data points indicating 50% RPE disruption are on or near the line; those with > 75% RPE disruption are at or above the threshold line. These relationships are most evident when the actual exposed retinal area is considered. These data suggest that there is reciprocity of exposure time and power for these wavelengths.

Discussion

Threshold Determination

To establish the threshold for RPE disruption at each wavelength, we implemented 2 different psychophysical procedures, a yes/no task and a 2AFC task. The 2AFC procedure has the advantage that it forces the grader to guess which image is the post-exposure image, which tends to protect the thresholds from criterion shifts that can influence yes/no task outcomes. Not surprisingly, 2AFC generates the same shape function but with slightly lower thresholds independent of the wavelength under test.

Minimum Visible Lesion Assessment

We acknowledge that there is no guarantee that RPE disruption corresponds to a complete loss of RPE cell integrity. According to the ANSI Z136.1-2022 light safety standard "the primary metric upon which the MPEs are based continues to be the presence of a minimum visible lesion (MVL) detected via ophthalmic examination after exposure" (ANSI Z136.1-2022 Appendix E1.3).[26] Much of the data for threshold determination included in safety standards do not incorporate histological analysis. Therefore, our data are consistent as a measurable change in the retina for light safety threshold. In fact, we consider that the use of cellular-scale retinal imaging in stabilized monkey eyes is a more sensitive, accurate, and precise measure of photochemical damage thresholds than clinical ophthalmoscopy.

Histological confirmation of these findings in the macaques used in this study is not possible. Nonetheless, our earlier publications[22,25] showed evidence of histological findings in macaques with RPE disruption. In whole-mounted and 6 µm paraffin sectioned macaque retina, exposure to 568 nm light with retinal radiant exposures of 788 J/cm^2 (approximately 4 times above the threshold for RPE disruption) showed visible disruption of the RPE layer

Table 3. Photochemical RPE Disruption Threshold and the Hill Slope (Steepness or Slope Factor) at the Testing Wavelengths

Wavelength (nm)	460	476	488	530	543	561	594	632	671
RPE disruption threshold (J/cm^2)	32.75	34.17	38.81	82.42	89.3	207.4	291.3	1120	4691.5
Hill slope *p*	0.161	0.192	0.156	0.10	0.031	0.033	0.021	0.0056	0.0007

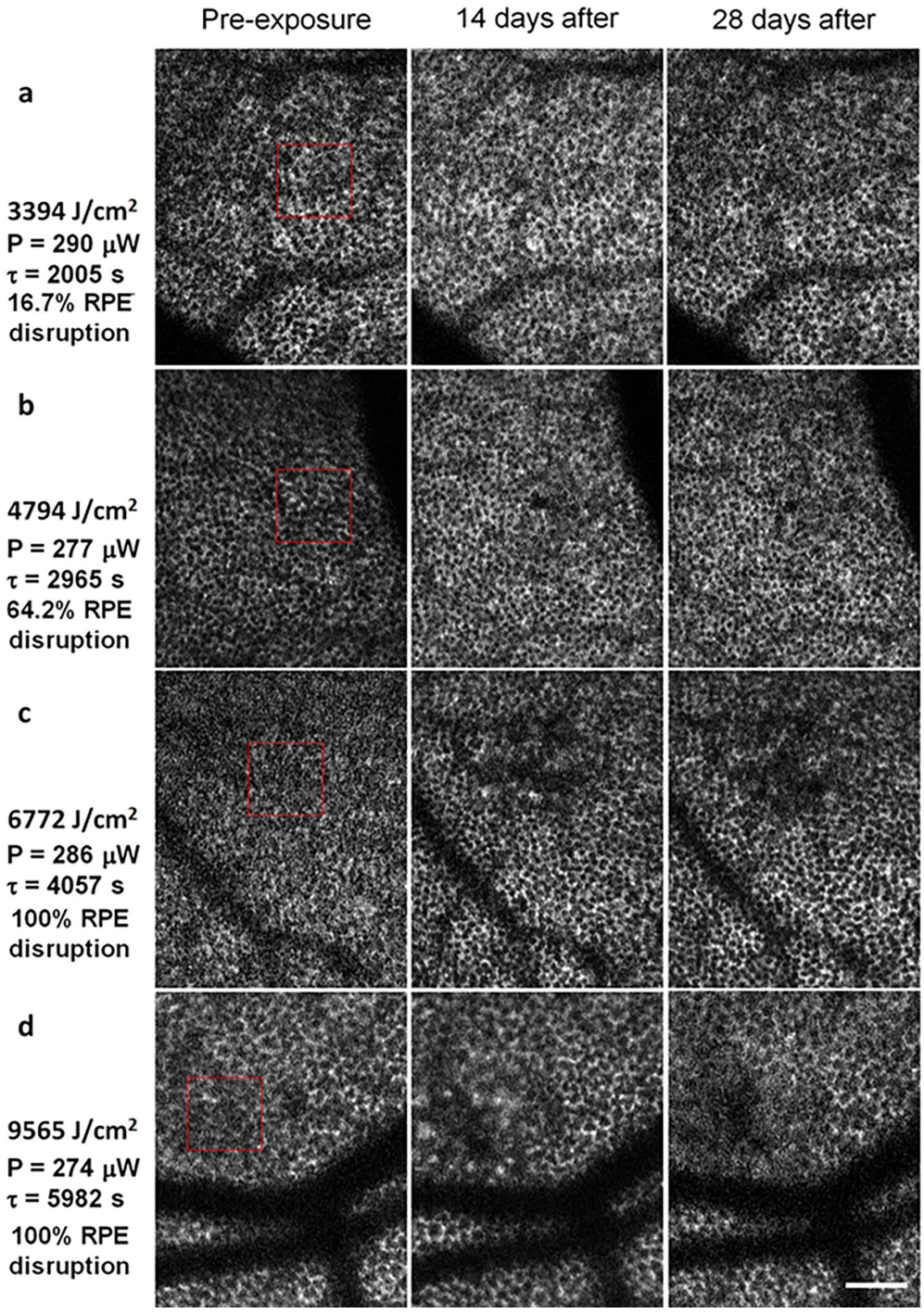

Figure 4. Pre-, 14, and 28 days post-exposure images of the RPE cells in locations exposed by uniform light exposure field at 671 nm with four RREs. (**a**) The 3394 J/cm^2 (290 µW for 2005 seconds), (**b**) 4794 J/cm^2 (277 µW for 2965 seconds), (**c**) 6772 J/cm^2 (286 µW for 4057 seconds), and (**d**) 9565 J/cm^2 (274 µW for 5982 seconds). The *red square* depicts the exposure locations. No visible change was detected at the site of 3394 J/cm^2 exposure. RPE disruption was observed starting at 2 weeks post-exposure for ≥ 4794 J/cm^2. Scale bar = 100 µm.

and cone outer segments. The near threshold exposure to 247 J/cm^2 (compared to the ED50 threshold of 207.4 J/cm^2 for 561 nm exposures reported here) was clearly visible in the wholemount but there were no obvious changes in the 6 µm section of retina.

We have also previously assessed the relationship between RPE disruption from 568 nm exposures and findings with clinical OCT and rhodopsin densitometry.[25] In clinical OCT (Heidelberg Spectralis HRA+OCT), a 0.5° lesion within a 16° B scan would impact only 19 A scans across the exposure region. Nonetheless, in regions of RPE disruption resulting from an RRE of 800 J/cm^2, there was a significant reduction in the separation of the inner/outer segment junction (or the ellipsoid zone) and the insertion of the

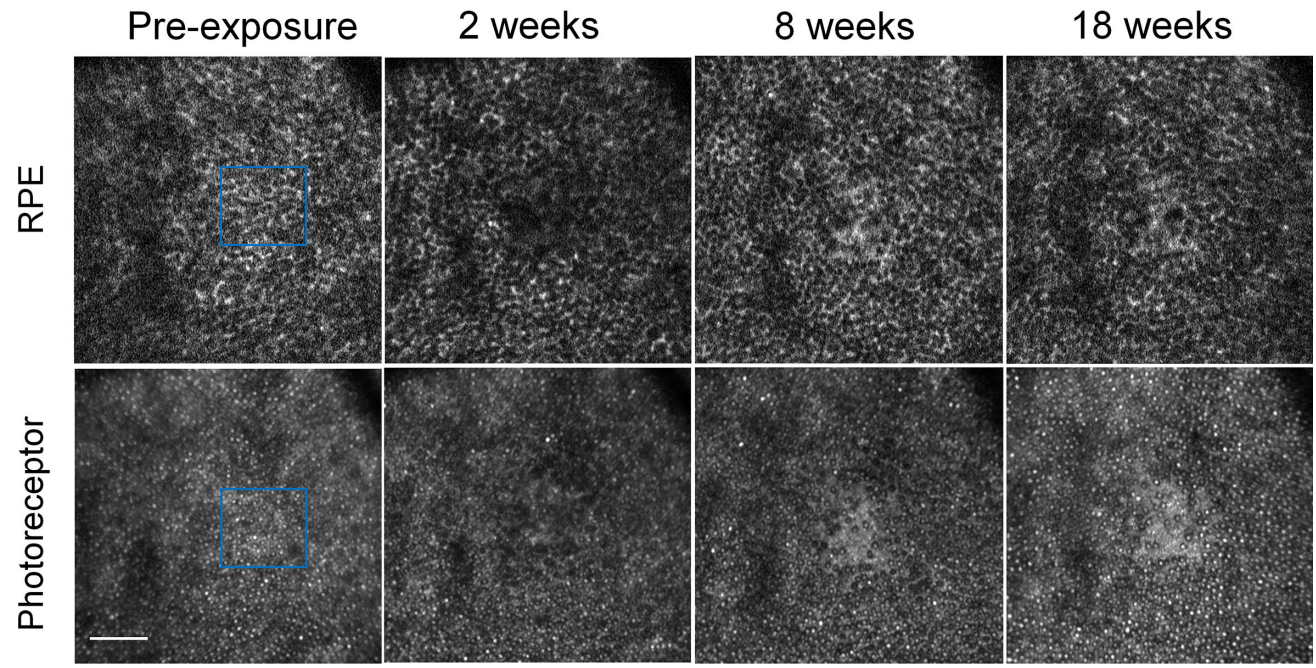

Figure 5. Pre-, 2, 8, and 18 weeks post-exposure images of both the RPE cells and photoreceptor mosaics in locations exposed by uniform light exposure field at 460 nm, with 34 J/cm^2 (140 µW for 42 seconds). The *blue square* indicates the exposure location. Both RPE and photoreceptor disruption was observed starting at 2 weeks post-exposure. Long-term cone photoreceptor outer segment loss was observed starting at 8 weeks and further confirmed at 18 weeks follow-up. Scale bar = 100 µm.

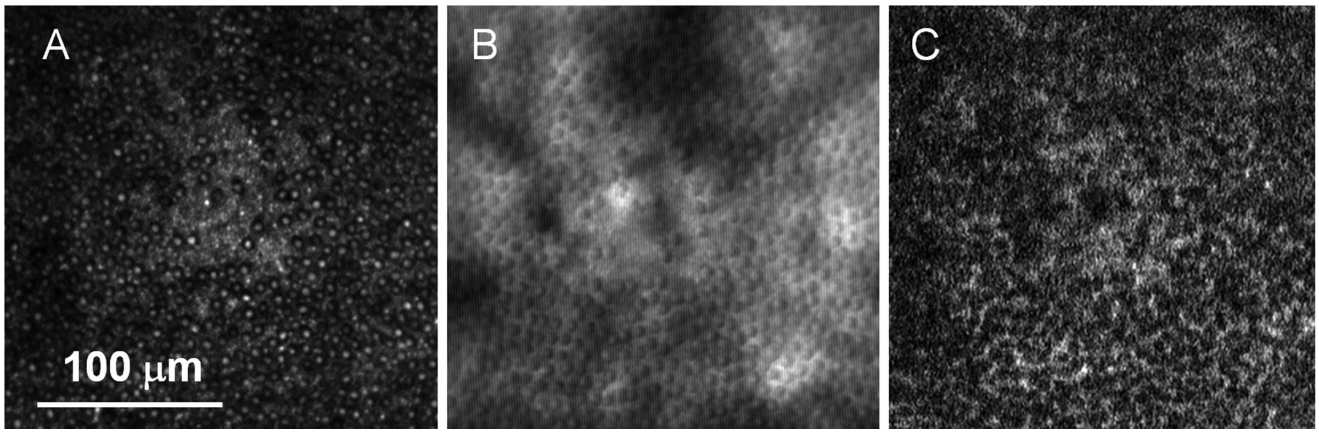

Figure 6. Structural imaging at 10 months follow-up after 460 nm exposure by (**a**) confocal, (**b**) offset aperture, (**c**) fluorescence AOSLO suggests long term cone loss and RPE disruption after a 460 nm exposure.

photoreceptors into the RPE (or the outer segment tips). However, there were no significant changes in the mean apparent density of photopigment or the initial rate of photopigment recovery from photobleaching (considered to be a correlate to retinal function). Higher light exposures displayed a significant reduction in mean apparent density of photopigment. At lower light levels (400 J/cm^2), approximately two times the threshold for RPE disruption, there were no notable differences measured with OCT or photopigment densitometry (although there was an unexplained, minimally significant, increase in mean apparent density of photopigment).

Based on these previously published results,[22,25] near threshold exposures for RPE disruption exhibit less disorganization of the photoreceptor outer segments and, in turn, less accumulation of cellular debris than more severe cases of RPE disruption. This may indicate that RPE function is not impacted by RPE disruption. Alternatively, it may be indicative of photoreceptors overlaying minimal visible lesions being serviced by healthy RPE cells in close proximity and surrounding the affected RPE cells. It is also possible that the sensitivity of the OCT and densitometry measurements were not sufficient to measure subtle changes in photoreceptor size and function. Although

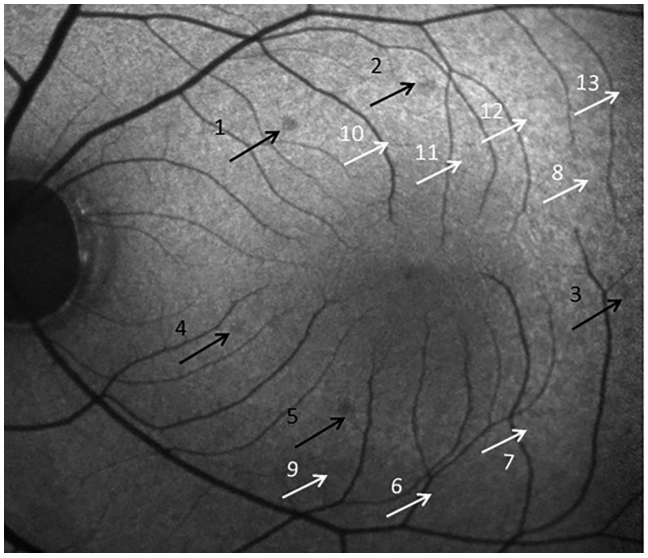

Figure 7. Blue-light autofluorescence of the M#2 retina at least 2 weeks (variable for each location) following 594 nm exposure. AF decrease (appeared as *dark dots* indicated by the *black arrows*) were observed at the site of exposure on or above 491 J/cm^2. No visible signal change was detected at the site of 348 J/cm^2 (location = 10-13) and 246 J/cm^2 (location = 6-9) exposure, as indicated by the *white arrows*.

unlikely, we cannot completely rule out that RPE disruption stems from local changes in the environment impacting the autofluorescence signal from the underlying RPE. These are potentially interesting questions that may be answered with recent advances in adaptive optics (AO)-OCT techniques but are outside the scope of this project. Nonetheless, the presence of RPE disruption meets the criteria for ophthalmoscopically minimal visible lesions for light safety considerations.

A Photochemical Damage Mechanism

Based on the exposure conditions, the retinal damage in this study would be from either photochemical or photothermal effects. Photothermal damage occurs immediately in response to a > 10°C increase in temperature. Such thermal effects did not occur with the exposures in this study. The temperature rise during exposure was calculated using a thermal model to be less than 1 K at all tested wavelengths.[27] In addition, photothermal damage appears right after the exposure, however, we did not observe any changes in the immediate post-exposure images beyond the expected AF reduction.[13] Photochemical damage is expected to be confined to the illumination field. However, regions of RPE disruption are often not the square shape of the illumination field and are occasionally larger. This is a consequence

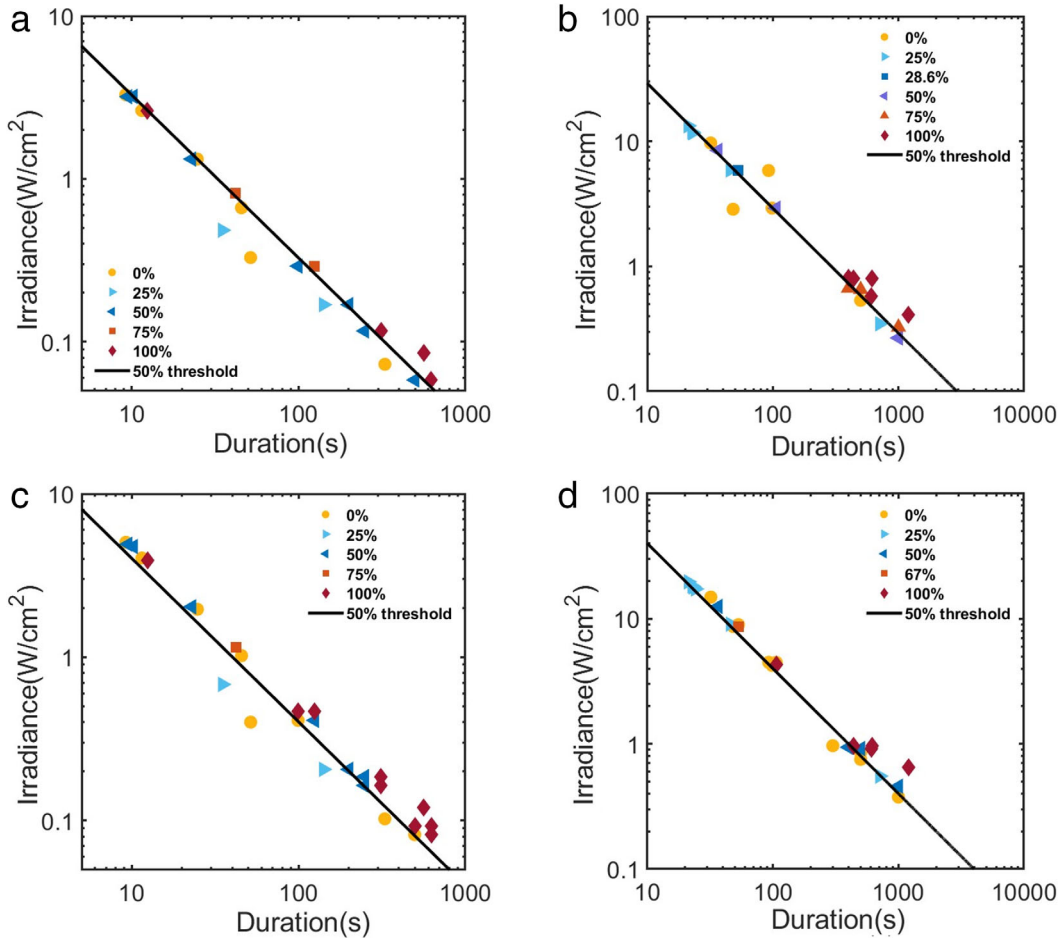

Figure 8. Reciprocity plots of irradiance versus exposure duration for (**a**) 460 nm and (**b**) 594 nm input light assuming an emmetropic monkey eye with a focal length of 15 mm. Reciprocity plots for irradiance calculated using the actual axial length of individual monkey eyes are also shown for (**c**) 460 nm and (**d**) 594 nm input light. In all plots, the *solid line* represents the established disruption threshold (Table 3). Data point color and shape indicate the percentage of locations showing RPE disruption.

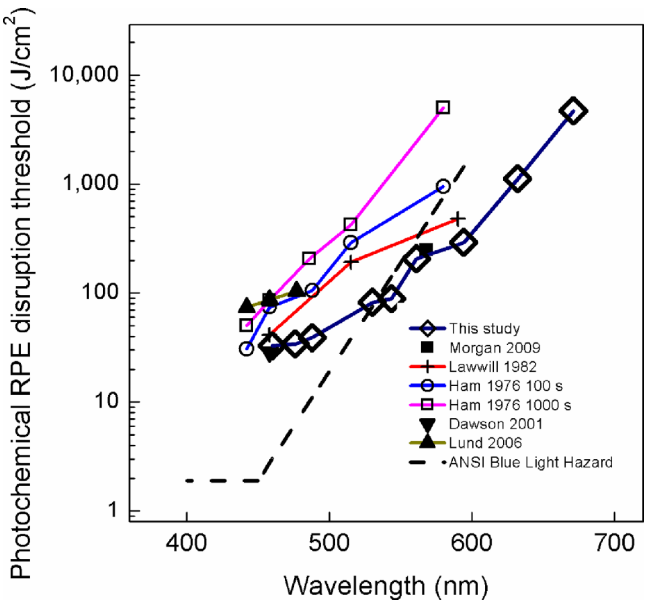

Figure 9. Comparison of the action spectrum for photochemical RPE disruption with previous data for minimum visible lesion threshold and the ANSI blue light hazard.[17,28] Exposure threshold levels are adjusted for direct comparison at the cornea.

of the natural ocular motion from heart rate and breathing during exposure leading to a less sharp border between exposed and unexposed RPE cells. Photochemical damage can occur when the rate of energy deposition related to the wavelength and exposure duration is too low to give rise to an appreciable temperature increase in the retina. The principle of reciprocity between the radiant flux (exposure power) and exposure duration is a hallmark of a photochemical damage mechanism. This reciprocity was observed for two of the tested wavelengths representing opposite ends of the visible spectrum. Therefore, we conclude that the damage observed under the conditions of our experiments was via a photochemical damage mechanism.

Light Safety

Cellular level imaging with FAOSLO and the stabilized exposure during imaging under anesthesia, as well as the 2AFC method for threshold determination, provided the most sensitive measure of the disruption threshold to date. We plotted the action spectrum as well as the previously published data for photochemical damage thresholds for minimal visible lesions reproduced from van Norren and Gorgels' compilation of data in Figure 9.[28] All the minimum visible lesion thresholds shown here were converted to the exposure irradiance level at the cornea, removing the ocular transmission function, if necessary. At the shortest wavelength tested, the threshold for RPE disruption is 32.75 J/cm^2 at 460 nm, which agreed well with Dawson's 28.57 J/cm^2 threshold at 458 nm. Previously in our laboratory, Morgan et al. observed permanent retinal RPE disruption at 568 nm using FAOSLO,[14] but we obtained the threshold for 561 nm RPE disruption at a slightly lower light exposure level in this study by testing RREs with smaller intervals and the application of 2AFC evaluation method. The measured photochemical RPE disruption threshold has a slope similar to the previous threshold data, but the measured thresholds are much below the thresholds established previously by Lawwill et al.,[29] Ham et al.,[30] and Lund et al.[23] in their earlier work. In this study, we measured the action spectrum for RPE disruption and observed only RPE disruption except for with the 460 nm exposures. This also indicated that action spectra for RPE disruption and photoreceptor damage are different. Apparently, the thresholds for photoreceptor damage are larger beyond 476 nm, which means that the slope of the action spectrum for photoreceptor damage should be steeper.

The ANSI blue light hazard[17] is also plotted in Figure 9 for direct comparison. We observed RPE photochemical disruption at 671 nm, extending the photochemical action spectrum close to the near infra-red (NIR) range. Our measured RPE disruption threshold is lower than the previous published result using traditional fundus imaging or histology. Compared with ANSI Z136.1-2014 section 8.3.2,[17] the RPE disruption threshold we obtained is only 3 times above the ANSI blue light hazard at 488 nm. This indicates that in the blue region of the spectrum, the ANSI standard is safe, but does not provide the order of magnitude of protection often assumed to be incorporated into the standard. At 594 nm, the measured threshold is 5 times smaller than the 2014 ANSI blue light hazard.[17] The measured photochemical RPE disruption threshold has a much shallower slope than the ANSI blue light hazard MPE and the 2 curves cross at approximately 530 nm, which indicates that the blue light hazard provides insufficient protection for laser and other light sources, especially at longer wavelengths and needs to be modified for better ocular protection from laser exposure. We recommend a new ocular MPE for the blue light hazard in the regime of 450 to 700 nm with a maximum retinal radiant exposure of $2.7 \times 10^{0.012(\lambda-450)}$ J/cm^2. This has been incorporated into the recently published ANSI Z136.1-2022 standard.[26] Overall, our study provides updated photochemical thresholds for visible light safety especially in ophthalmic settings, such as endoilluminator, operating microscope, fundus imaging, and visible-light OCT or AF imaging.

Conclusions

We delivered exposures with different RREs at nine wavelengths across the visible spectrum into four living monkeys' retinas to measure the action spectrum for photochemical RPE disruption threshold. By using an FAOSLO, preexposure, immediately, 2 and 4 weeks post-exposure RPE images were captured, aligned, and characterized to analyze the exposure outcomes. We tested our results with the 2AFC method to evaluate the RPE disruption at individual locations. For each wavelength, a probit fitting was used to accurately measure the 50% threshold for photochemical RPE disruption and generate an action spectrum. We found that photochemical RPE disruption thresholds are slightly lower than published thresholds. Further photochemical RPE disruption extends to longer wavelengths than previously observed. The action spectrum is considerably shallower than the spectral dependence of the traditional ANSI blue light hazard, emphasizing the need for more caution with increasing wavelength than previously published data. The mechanism for photochemical RPE disruption remains unknown, pending experiments that measure the action spectrum for RPE disruption caused by individual molecular species.

Investigative Ophthalmology & Visual Science

Acknowledgments

The authors thank Lee Anne Schery, Amber Walker, Jennifer Strazzeri, Qiang Yang, Marty Gira, Keith Parkins, William S. Fischer, Ebrahim Aboualizadeh, and all the graders for their assistance. The authors would also like to thank Robert Thomas and Chad Oian for their effort on thermal simulations. The authors thank Michael Boulton and Janet Sparrow, for their valuable discussion on the photochemical RPE disruption mechanism. The authors would also like to thank David Sliney for input on the experiment design and Francois Delori for interpretation of ANSI Z136.1-2014 and its application for ocular exposures.

Supported by the National Institute of Health (Bethesda, MD, USA) through the Grants R01-EY004367, P30-EY001319, and an unrestricted grant from the Research to Prevent Blindness (RPB) Foundation to the Flaum Eye Institute. The image registration software used to produce our AOSLO images, DeMotion, was developed by Alfredo Dubra and Zach Harvey with funding from Research to Prevent Blindness (New York, NY, USA) and the National Institute of Health through the Grants BRP-EY014375 and 5 K23 EY016700. Alfredo Dubra and Kamran Ahmad developed the adaptive optics control software.

Disclosure: **J. Zhang**, Canon, Inc. (F, P), University of Rochester (P), Robotrak Technologies Co., Ltd. (O, P); **R. Sabarinathan**, None; **T. Bubel**, None; **W. Jia**, None; **D.R. Williams**, Canon Inc. (F, R), University of Rochester (P); **J.J. Hunter**, University of Rochester (P)

References

1. Green WR, Robertson DM. Pathologic findings of photic retinopathy in the human eye. *Am J Ophthalmol*. 1991; 112(5):520–527.
2. Hope-Ross M, Travers S, Mooney D. Solar retinopathy following religious rituals. *Br J Ophthalmol*. 1988;72(12): 931–934.
3. Hupp SL. Delayed, incomplete recovery of macular function after photic retinal damage associated with extracapsular cataract extraction and posterior lens insertion. *Arch Ophthalmol*. 1987;105(8):1022–1023.
4. Khwarg SG, Linstone FA, Daniels SA, et al. Incidence, risk factors, and morphology in operating microscope light retinopathy. *Am J Ophthalmol*. 1987;103(3, Part 1):255–263.
5. Michels M, Lewis H, Abrams GW, Han DP, Mieler WF, Neitz J. Macular phototoxicity caused by fiberoptic endoillumination during pars plana vitrectomy. *Am J Ophthalmol*. 1992;114(3):287–296.
6. Yannuzzi LA, Fisher YL, Krueger A, Slakter J. Solar retinopathy: a photobiological and geophysical analysis. *Trans Am Ophthalmol Soc*. 1987;85:120–158.
7. Uniat L, Olk RJ, Hanish SJ. Welding arc maculopathy. *Am J Ophthalmol*. 1986;102(3):394–395.
8. Byrnes GA, Chang B, Loose I, Miller SA, Benson WE. Prospective incidence of photic maculopathy after cataract surgery. *Am J Ophthalmol*. 1995;119(2):231–232.
9. Yanagi Y, Iriyama A, Jang WD, Kadonosono K. Evaluation of the safety of xenon/bandpass light in vitrectomy using the A2E-laden RPE model. *Graefe's Arch Clin Exp Ophthalmol*. 2007;245(5):677–681.
10. Mainster MA, Findl O, Dick HB, et al. The blue-light-hazard vs. blue-light-hype. *Am J Ophthalmol*. 2022;240:51–57.
11. Cougnard-Gregoire A, Merle BMJ, Aslam T, et al. Blue light exposure: ocular hazards and prevention—a narrative review. *Ophthalmol Ther*. 2023;12(2):755–788.
12. Morgan JIW, Dubra A, Wolfe R, Merigan WH, Williams DR. In vivo autofluorescence imaging of the human and macaque retinal pigment epithelial cell mosaic. *Invest Ophthalmol Vis Sci*. 2009;50(3):1350–1359.
13. Morgan JIW, Hunter JJ, Merigan WH, Williams DR. The reduction of retinal autofluorescence caused by light exposure. *Invest Ophthalmol Vis Sci*. 2009;50(12):6015–6022.
14. Morgan JI, Hunter JJ, Masella B, et al. Light-induced retinal changes observed with high-resolution autofluorescence imaging of the retinal pigment epithelium. *Invest Ophthalmol Vis Sci*. 2008;49(8):3715–3729.
15. American National Standards Institute (ANSI) Z136.1-2007 - American National Standard for Safe Use of Lasers. Accessed November 1, 2023. Available at: https://webstore.ansi.org/standards/lia/ansiz1362007.
16. Hunter JJ, Morgan JIW, Merigan WH, Williams DR. *Retinal phototoxicity observed using high-resolution autofluorescence imaging*. In: Melville, NY: AIP Publishing; 2009:61–65.
17. American National Standards Institute (ANSI) Z136.1-2014 - American National Standard for Safe Use of Lasers. Accessed November 1, 2023. Available at: https://webstore.ansi.org/standards/lia/ansiz1362014.
18. Hunter JJ, Masella B, Dubra A, et al. Images of photoreceptors in living primate eyes using adaptive optics two-photon ophthalmoscopy. *Biomed Opt Express, BOE*. 2011;2(1):139–148.
19. Burns SA, Tumbar R, Elsner AE, Ferguson D, Hammer DX. Large-field-of-view, modular, stabilized, adaptive-optics-based scanning laser ophthalmoscope. *J Opt Soc Am A, JOSAA*. 2007;24(5):1313–1326.
20. Yang Q, Zhang J, Nozato K, et al. Closed-loop optical stabilization and digital image registration in adaptive optics scanning light ophthalmoscopy. *Biomed Opt Express, BOE*. 2014;5(9):3174–3191.
21. Zhang J, Yang Q, Saito K, Nozato K, Williams DR, Rossi EA. An adaptive optics imaging system designed for clinical use. *Biomed Opt Express, BOE*. 2015;6(6):2120–2137.
22. Hunter JJ, Morgan JI, Merigan WH, Sliney DH, Sparrow JR, Williams DR. The susceptibility of the retina to photochemical damage from visible light. *Prog Retinal Eye Res*. 2012;31(1):28–42.
23. Lund DJ, Stuck BE, Edsall P. Retinal injury thresholds for blue wavelength lasers. *Health Phys*. 2006;90(5):477–484.
24. Paques M, Simonutti M, Roux MJ, et al. High resolution fundus imaging by confocal scanning laser ophthalmoscopy in the mouse. *Vision Res*. 2006;46(8–9):1336–1345.
25. Masella BD, Hunter JJ, Williams DR. Rod photopigment kinetics after photodisruption of the retinal pigment epithelium. *Invest Ophthalmol Vis Sci*. 2014;55(11):7535–7544.
26. American National Standards Institute (ANSI) Z136.1-2022 – American National Standard for Safe Use of Lasers. Accessed November 1, 2023. Available at: https://webstore.ansi.org/standards/lia/ansiz1362022.
27. Oian CA, Zhang J, Thomas RJ, Hunter JJ. *Estimation of retina thermal response in photochemical damage studies*. In: Melville, NY: AIP Publishing; 2017:151–156.
28. van Norren D, Gorgels TGMF. The action spectrum of photochemical damage to the retina: a review of monochromatic threshold data. *Photochem Photobiol*. 2011;87(4):747–753.
29. Lawwill T. Three major pathologic processes caused by light in the primate retina: a search for mechanisms. *Trans Am Ophthalmol Soc*. 1982;80:517–579.
30. Ham WT, Mueller HA, Ruffolo JJ, Guerry D, Guerry RK. Action spectrum for retinal injury from near-ultraviolet radiation in the aphakic monkey. *Am J Ophthalmol*. 1982;93(3):299–306.

Investigative Ophthalmology & Visual Science